Clim Dyn (2013) 40:1467–1481
DOI 10.1007/s00382-012-1340-1

Spring asymmetric mode in the tropical Indian Ocean: role of El Niño and IOD

Soumi Chakravorty · J. S. Chowdary · C. Gnanaseelan

Received: 20 December 2011 / Accepted: 12 March 2012 / Published online: 5 April 2012

Abstract The spring asymmetric mode over the Tropical Indian Ocean (TIO) is characterized by contrasting patterns of rainfall and surface wind anomalies north and south of Equator. The asymmetric pattern in rainfall has evolved as a leading mode of variability in the TIO and is strongly correlated with El Niño-Southern Oscillation (ENSO) and positive Indian Ocean Dipole (IOD). The evolution of the asymmetric pattern in rainfall and surface wind during pure El Niño/IOD and co-occurrence years are examined in the twentieth century reanalysis for the period of 1871–2008 and atmospheric general circulation model (AGCM) simulations. The study revealed that spring asymmetric mode is well developed when El Niño co-occurred with IOD (positive) and is driven by the associated meridional gradients in sea surface temperature (SST) and sea level pressure (SLP). The pure El Niño composites are characterized by homogeneous (spatially) SST anomalies (positive) and weaker SLP gradients and convection, leading to weak asymmetric mode. The asymmetric mode is absent in the pure IOD (positive) composites due to the persistence of east west SST gradient for a longer duration than the co-occurrence years. The meridional gradient in SST anomalies over the TIO associated with the ENSO-IOD forcing is therefore crucial in developing/strengthening the spring asymmetric mode. The northwest Pacific anticyclonic circulation further strengthen the asymmetric mode in surface winds by inducing northeasterlies in the north Indian Ocean during pure El Niño and co-occurrence years. The simulations based on AGCM, forced by observed SSTs during the period of 1871–2000 supported the findings. The analysis of available station and ship track data further strengthens our results.

Keywords ENSO · IOD · Tropical Indian Ocean · Northwest Pacific anticyclone · Spring asymmetric mode

S. Chakravorty · J. S. Chowdary · C. Gnanaseelan (✉)
Indian Institute of Tropical Meteorology, Pune 411008, India
e-mail: seelan@tropmet.res.in

1 Introduction

Tropical oceans are dominated by unstable ocean–atmosphere coupled interactions such as El Niño-Southern Oscillation (ENSO) over the Pacific Ocean and Indian Ocean Dipole (IOD; Saji et al. 1999; Webster et al. 1999; Murtugudde et al. 2000) over the Indian Ocean. El Niño induces a basin-wide wintertime (hereafter, seasons refer to those for the northern hemisphere) surface warming in the Tropical Indian Ocean (TIO), known as Indian Ocean Basin mode (IOBM, Klein et al. 1999; Yang et al. 2007; Chowdary and Gnanaseelan 2007). This warming is mainly induced by the atmospheric teleconnections associated with El Niño (Klein et al. 1999; Lau and Nath 2000; Alexander et al. 2002) and also through ocean dynamics (Masumoto and Meyers 1998; Chambers et al. 1999; Xie et al. 2002).

Sea surface temperature (SST) anomalies (SSTA) associated with El Niño decay rapidly in spring over the eastern Pacific, but El Niño induced TIO warming persists up to the following August–September (Nigam and Shen 1993; Klein et al. 1999; Xie et al. 2009). The interannual surface heat flux variability is the dominant mechanism for the El Niño induced warming in most of the TIO (Klein et al. 1999; Alexander et al. 2002; Lau and Nath 2003; Tokinaga and Tanimoto 2004; Shinoda et al. 2004) except the southwest TIO. Ocean dynamics in the form of westward propagating downwelling Rossby waves play an

important role in controlling SST warming in the southwest TIO (Perigaud and Delecluse 1993; Masumoto and Meyers 1998; Chambers et al. 1999; Xie et al. 2002; Chowdary et al. 2009). Du et al. (2009) supported this by carrying out mixed layer heat budget analysis. The TIO surface warming pattern during the pure El Niño years is different from that of El Niño and IOD (positive) co-occurrence years (Chowdary and Gnanaseelan 2007, hereafter co-occurrence years). Strong westward propagation of downwelling Rossby waves is observed in the southern TIO during the co-occurrence years, but they are weak in the case of pure El Niño years. During pure El Niño years surface heat flux plays a dominant role in SST variability in TIO, whereas ocean dynamics play a major role in the variability during the IOD years. In the case of co-occurrence years both downwelling Rossby waves (confined only to southern TIO) and heat fluxes associated with ENSO are responsible for the TIO warming.

During boreal spring, asymmetric patterns in rainfall and winds develop over the TIO around the equator during the decay phase of El Niño (Kawamura et al. 2001; Wu et al. 2008; Xie et al. 2009; Du et al. 2009; Wu and Yeh 2010). Figure 1 shows the asymmetric pattern of spring 1998 with northeasterlies in north and northwesterlies in south of the equator. The 1997–1998 El Niño is recognized as the strongest event on instrumental records and the associated anomalies persist through the following summer, especially in the TIO. The basin-wide TIO warming is strong with mean warming of 0.7 °C in March–April. In general the variability associated with asymmetric mode enhances ENSO teleconnections to the TIO (Wu et al. 2008). Understanding the development of this mode is essential because it can give the precursory signals of the following monsoon by changing the land ocean temperature contrast and altering cloud cover, tropical rainfall and soil moisture in spring (Kawamura et al. 2001). El Niño thus can affect the following Asian summer monsoon through this asymmetric mode (Xie et al. 2010; Huang et al. 2010; Chowdary et al. 2010).

Kawamura et al. (2001) showed that the equatorial asymmetry in surface heat flux via positive wind-evaporation-SST (WES) feedback (Xie and Philander 1994) is responsible for generating the asymmetric mode in convection and SST over the TIO. Whereas, Wu et al. (2008) showed that the cross equatorial SST gradient due to the southwest TIO warming during October–November (ON) and north Indian Ocean cooling during December–January (DJ) are responsible for the initiation of the asymmetric mode. The persistence of the SST gradient over the TIO maintains this mode until April–May (AM). The spring asymmetric mode is highly correlated with preceding IOD (September–November; SON) and Niño 3.4 (December–February; DJF) indices (Wu et al. 2008). The importance of El Niño and IOD forcing on the formation of asymmetric mode is therefore addressed by the previous studies though the individual contributions are not known.

On the other hand over the northwest Pacific, an anomalous high pressure system with an anticyclonic surface circulation begins to appear in the lower troposphere during the mature phase (winter) of ENSO. The central/eastern Pacific warming helps to set up a favorable large scale environment for establishment and maintenance of northwest Pacific anticyclone through effective air–sea interaction (Wang et al. 2000; Lau and Nath 2003). The central Pacific warming in winter generates the equatorward flow to the west of the warming (Wang et al. 2000) which strengthen the mean northeasterlies in the Northern Hemisphere, which in turn intensify the evaporative cooling in the northwest Pacific. This SST cooling generates an anticyclone to the west of it due to Rossby wave response of suppressed convective heating (Wang et al. 2000). During the peak phase of northwest Pacific anticyclone (spring), the surface high and wind anomaly are originated and maintained by the positive thermodynamic feedback of local negative SST anomalies, suggestive of a local ocean–atmosphere interaction (Wang et al. 2000; Lau and Nath 2003).

During the decay phase of El Niño, evolution of SST anomalies in the TIO is different when El Niño occurs independently and co-occurs with IOD. This strongly suggests the possibility of different mechanisms driving the SST warming. Therefore, it is important to understand the role of El Niño and/or IOD forcing in developing spring asymmetric mode. Previous studies did not address these issues and were also limited to the recent years (period after 1950). In this context the present study examined the evolution of spring asymmetric mode for the past 138 years using the twentieth century reanalysis (Compo et al. 2011) data and atmospheric model simulations. Our observational and model results reveal that spring asymmetric mode in wind and precipitation pattern over the TIO is well developed when El Niño co-occurred with IOD, mainly due to meridional SST and sea level pressure (SLP) gradients. SST anomalies display very weak meridional gradient in pure El Niño composites and therefore a weaker asymmetric mode during the pure El Niño years. The different datasets and model used in the study are described in Sect. 2. Section 3 presents winter and spring EOF modes associated with the asymmetric pattern. Section 4 discusses the evolution of spring asymmetric mode in pure El Niño, IOD and co-occurrence composites. Atmospheric model simulations are discussed in Sect. 5 and analysis of station and ship track data is presented in Sect. 6. Section 7 provides a comprehensive summary.

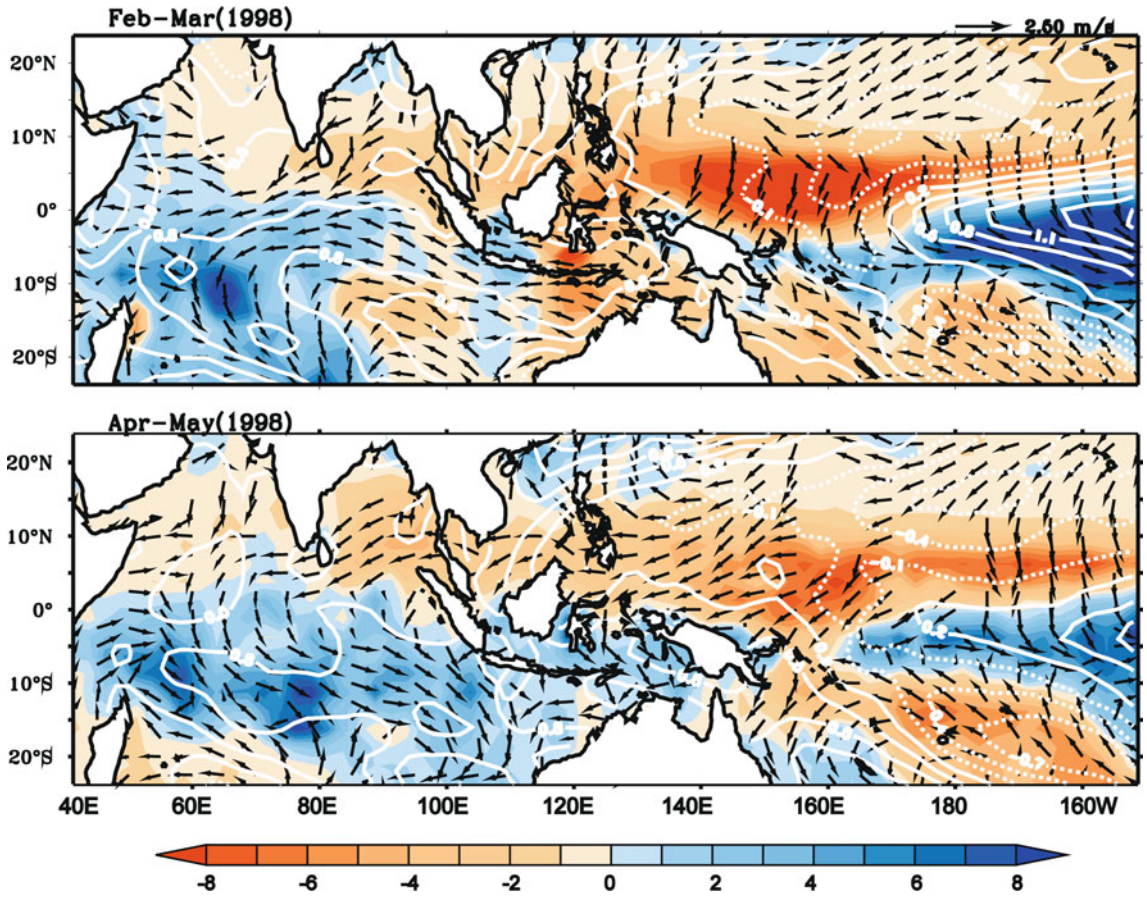

Fig. 1 Precipitation anomalies (*shaded*, mm day^{-1}) overlaid with SSTA (*contours*, °C) and surface wind anomalies (*vectors*, ms^{-1}) during **a** February–March 1998, **b** April–May 1998

2 Data and methodology

We mainly use the National Oceanic and Atmospheric Administration (NOAA) Extended Reconstructed SST (ERSST) product (Smith and Reynolds 2004) and the twentieth century reanalysis (20CR; Compo et al. 2011) for our analysis. Niño 3.4 index is computed as the SST anomalies of the central equatorial Pacific (5°S to 5°N, 170°W to 120°W) and Dipole Mode Index (DMI) is computed as the difference between western equatorial Indian Ocean (10°S to 10°N, 50°E to 70°E) and south-eastern equatorial Indian Ocean (10°S to Equator, 90°E to 110°E) SST anomalies. The El Niño and IOD events are classified as in Meyers et al. (2007). The list of El Niño and IOD events is provided in Table 1. It is observed that during the last 140 years, El Niño and positive IOD (IOD) events co-occurred 10 times, El Niño only (pure El Niño) events developed 15 times and IOD only (pure IOD) events developed 16 times. Observed station (e.g., Seychelles and Colombo) rainfall data for nineteenth century is obtained from the NOAA. In addition to these, we used the gridded dataset of monthly land precipitation of Dai et al. (1997) for the period 1850–1995 and the Center for Climate Prediction merged analysis for precipitation (CMAP; Xie and Arkin 1996) data for the period of 1979–2009. The frequent ship lanes surface marine data over the north Indian Ocean from the mouth of Gulf of Eden to Malacca Straits is also used for the analysis. The physical mechanisms associated with the asymmetric mode are studied by using empirical orthogonal function (EOF), composite and correlation analysis techniques.

In addition to the observational analysis, we used a 5 member ensemble mean of an atmospheric general circulation model (AGCM), which is T85 TOGA (Tropical Ocean Global Atmosphere), forced by tropical (20°N–20°S) interannual SSTs (Hurrell et al. 2008) from January 1871 through September 2001 (http://www.cesm.ucar.edu). The ensemble members differ only in their initial conditions (Collins et al. 2006). The model incorporates the climatological seasonal cycle of SSTs poleward of 30° latitude and linearly interpolates between 20° and 30°. The AGCM is the National Center for Atmospheric Research (NCAR) Community Atmospheric Model version 3 (CAM3) (Collins et al. 2006). Anomalies are calculated

Table 1 List of pure El Niño, pure IOD and El Niño and IOD co-occurrence years classified based on Meyers et al. (2007) (with a higher level of certainty)

Pure El Niño	Co-occurrence	Pure IOD
1877, 1888, 1899, 1911, 1914, 1940, 1965, 1986, 1987, 1991, 2002, 2004	1896, 1902, 1905, 1923, 1963, 1972, 1982, 1997, 2006	1885, 1887, 1891, 1894, 1919, 1926, 1935, 1944, 1945, 1946, 1961, 1967, 1994

based on the monthly mean climatology of 1871–2000. Linear trends of all the time series are removed to eliminate the decadal and longer time scale variations. Three monthly smoothing (running mean) is applied for all variables to remove the intraseasonal variability. This AGCM has successfully simulated the ENSO-teleconnections to the Indian Ocean region and their interdecadal modulation (Chowdary et al. 2012). Coupled multi-model ensemble showed significant skill in predicting the spring asymmetric mode at 1 month lead (Chowdary et al. 2010).

3 Leading modes of spring variability in the TIO

To understand the leading modes of variability during February–March (FM) and AM over the TIO, EOF analysis is carried out on CMAP bimonthly (mean) precipitation anomalies. Anomalous asymmetric pattern in precipitation over the TIO has emerged as the second mode of variability during FM (Fig. 2a) with 18 % variance (EOF-1 has 23 % variance), whereas it emerged as the leading EOF mode in AM (Fig. 2b) with 21 % variance (EOF-2 has 12 % variance). The precipitation anomalies are significantly positive over the southern TIO and negative over the Bay of Bengal (BOB) during FM, indicating a strong asymmetric mode. This asymmetric mode is well organized over the entire TIO in AM. The surface wind anomalies (vectors) regressed against the corresponding precipitation PCs are shown in Fig. 2a and b. Anomalous asymmetric pattern in surface winds (northeasterlies north of equator and northwesterlies south of equator) associated with the rainfall is dominant over the entire basin. The correlation coefficient (CC) between the FM precipitation PC-2 (PC-1) and November–January (NDJ) Niño 3.4 is 0.71 (0.23) and that with ON DMI is 0.55 (0.15) respectively. The corresponding CC for the AM precipitation PC-1 (PC-2) is 0.73 (0.06) with NDJ Niño 3.4 and 0.5 (0.25) with ON DMI. Hereafter, we denote seasons during the developing and decay years of El Niño with (0) and (1) respectively.

Similar to surface winds, SST and SLP anomalies are also regressed upon the precipitation PCs (Fig. 2c, d). North south gradient in SLP anomalies with positive in the north and negative in the south and SST anomalies (weak negative in the north and positive in the south) are observed in FM. In AM, meridional gradient in SST anomaly weakened without much changes in the southern warming. On the other hand north–south gradient in SLP anomalies is much more prominent during AM (Fig. 2d). Above discussions reveal that asymmetric mode is the dominant interannual variability over the TIO and is highly correlated with El Niño and IOD indices. It is therefore important to understand the relative role of El Niño/IOD in

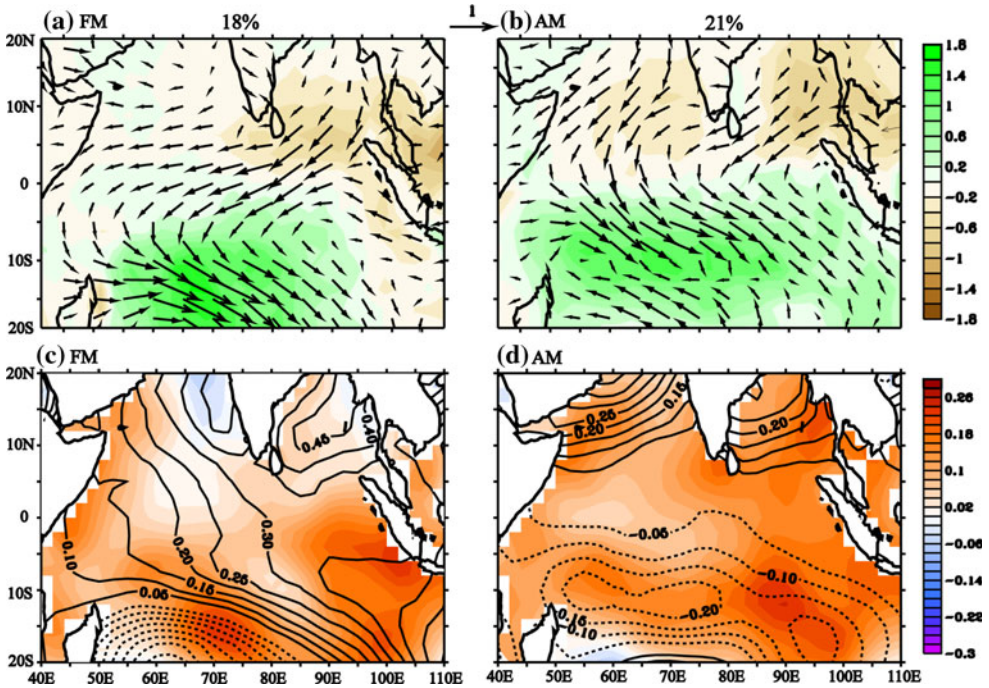

Fig. 2 The spatial pattern of the EOF modes of observed precipitation anomalies for the period of 1979–2009 (*shaded*, *top panels*) **a** February–March (2nd mode, 18 % variability) and **b** April–May (1st mode, 21 % variability) overlaid with the surface wind anomaly regressed upon respective precipitation principal component (*vectors*). *Bottom panels* are SST (*shaded*) and SLP anomalies (*contour*), regressed with precipitation PCs during **c** February–March and **d** April–May. The variance explained by the EOF mode is shown at the *top* of the respective *panels*

developing the anomalous asymmetric mode in rainfall and low level circulation over the TIO during late winter and spring.

4 Evolution of spring asymmetric mode

Figure 3 illustrates the bimonthly composite of SST and surface wind anomalies for pure El Niño (left panel), El Niño and IOD co-occurrence (middle panel) and pure IOD (right panels) years from ON(0) to June–July(1) (JJ(1)). SST warming over the TIO during pure El Niño years is almost homogeneous in space from DJ(0/1) to JJ(1) (Fig. 3a–e). Surface winds are easterlies over most of the TIO from ON(0) to FM(1). TIO exhibits asymmetric mode with weak northeasterlies north of the equator and weak northwesterlies confining only to the southwest during AM(1). This circulation pattern is much more organized in summer. On the other hand, over the northwest Pacific, surface anticyclonic circulation in response to El Niño began to appear in ON(0). The anomalous anticyclonic circulation first appeared in the region south of Philippines prior to the peak phase of El Niño, which migrates slowly toward north and centered around 10°N by winter (Fig. 3). This persists up to JJ(1) and is in agreement with Wang et al. (2000), Xie et al. (2009) and Chowdary et al. (2010). Cold SST anomalies are noticed in most of the western Pacific region in ON(0) mainly due to the intensification of prevailing northeasterly trades by WES feedback and generation of upwelling Rossby waves (Wang et al. 2000). During spring northeasterly wind anomalies extend from northwest Pacific to north Indian Ocean. This strongly supports the possible influence of northwest Pacific circulation on TIO.

The TIO SST warming is stronger during the co-occurrence years compared to pure El Niño or IOD years (Fig. 3) with prominent basin wide warming from DJ(0/1) to FM(1). SST anomalies exhibit east–west dipole like pattern with negative anomalies in the east Equatorial Indian Ocean and positive anomalies in the west during ON(0) (Fig. 3f) during the co-occurrence years. Warming over the TIO is not homogeneous during co-occurrence years and the maximum warming is located over the southwest TIO and this persists until the early summer. Whereas the north Indian Ocean (in particular the Arabian Sea) cools during ON(0) to AM(1) with a peak cooling in FM(1). This stronger SST anomalies during the co-occurrence years is mainly responsible for the strong winds over Indian Ocean. Asymmetric wind pattern appears in FM(1) which is prominent in AM(1) but weaken thereafter (Figs. 3h–j). Note that this spring asymmetric mode in wind pattern is stronger during co-occurrence years compared to pure El Niño years. It is important to note that the northeasterly wind anomalies first initiates over western Pacific in FM(1) during co-occurrence years which extend from dateline to Arabian Sea during AM(1). This is mainly responsible for the early decay (AM(1)) of the eastern Pacific warm SST anomalies in co-occurrence case (figure not shown). This is not the case for pure El Niño composite (Fig. 3d, i). The role of eastern/central Pacific SST anomalies is also examined to further strengthen our study. It is important to note that the stronger eastern Pacific warming during the co-occurrence years intensify the northwest Pacific cooling as compared to pure El Niño years in FM(1). This strong cooling strengthens the thermodynamic feedback and intensifies the anticyclone in spring during co-occurrence years. The resulting strong easterly wind anomalies in the north Indian Ocean region strengthen the asymmetric wind pattern in spring. The intensity and position of northwest Pacific anticyclone strengthen the northeasterlies over north Indian Ocean. In short the meridional gradient in TIO SST anomalies and northwest Pacific anticyclone appears to be important for developing the asymmetric mode. During pure IOD years east–west gradient in SST anomalies over the equatorial Indian Ocean along with anomalous surface easterlies are evident in ON(0) to the following spring (Fig. 3). SST and wind anomalies are weak over TIO and northwest Pacific region from DJ(0/1) to JJ(1) compared to the other two composites. This suggests that IOD alone can not initiate asymmetric wind pattern over the TIO. However, El Niño induced basin scale warming is super imposed on the IOD forced southwest TIO warming during the co-occurrence years resulting strong meridional SST gradient. Therefore, IOD plays a key role in the evolution of asymmetric pattern (in winds) during the co-occurrence years by strengthening the southern TIO Rossby waves.

Figure 4 shows the bimonthly composite of SLP and 850 hPa wind anomalies from DJ(0/1) to JJ(1). Associated with anomalous anticyclonic circulation, SLP anomalies are positive over the Philippines Sea/northwest Pacific in all seasons starting from DJ(0/1) in both pure El Niño and co-occurrence composites. This high pressure anomaly is very weak during pure IOD years (Figs. 4i–l). Another SLP high associated with anomalous anticyclonic circulation is located over the southeast TIO during pure El Niño and co-occurrence years in DJ(0/1) and FM(1). Both the anticyclones are resulting from the Rossby type response to symmetric heating (Gill 1980) about the equator for both pure El Niño and co-occurrence years. The anticyclones (both north and south of the equator), however, appear to induce strong easterly wind anomalies over the equatorial Indian Ocean along with SST forcing in winter. SLP high and anticyclonic circulation anomalies in the southeast TIO persist up to late spring (AM(1)) during pure El Niño events (Fig. 4c), resulting a weak meridional SLP gradient. This gradient strengthen by JJ(1). It is interesting to note

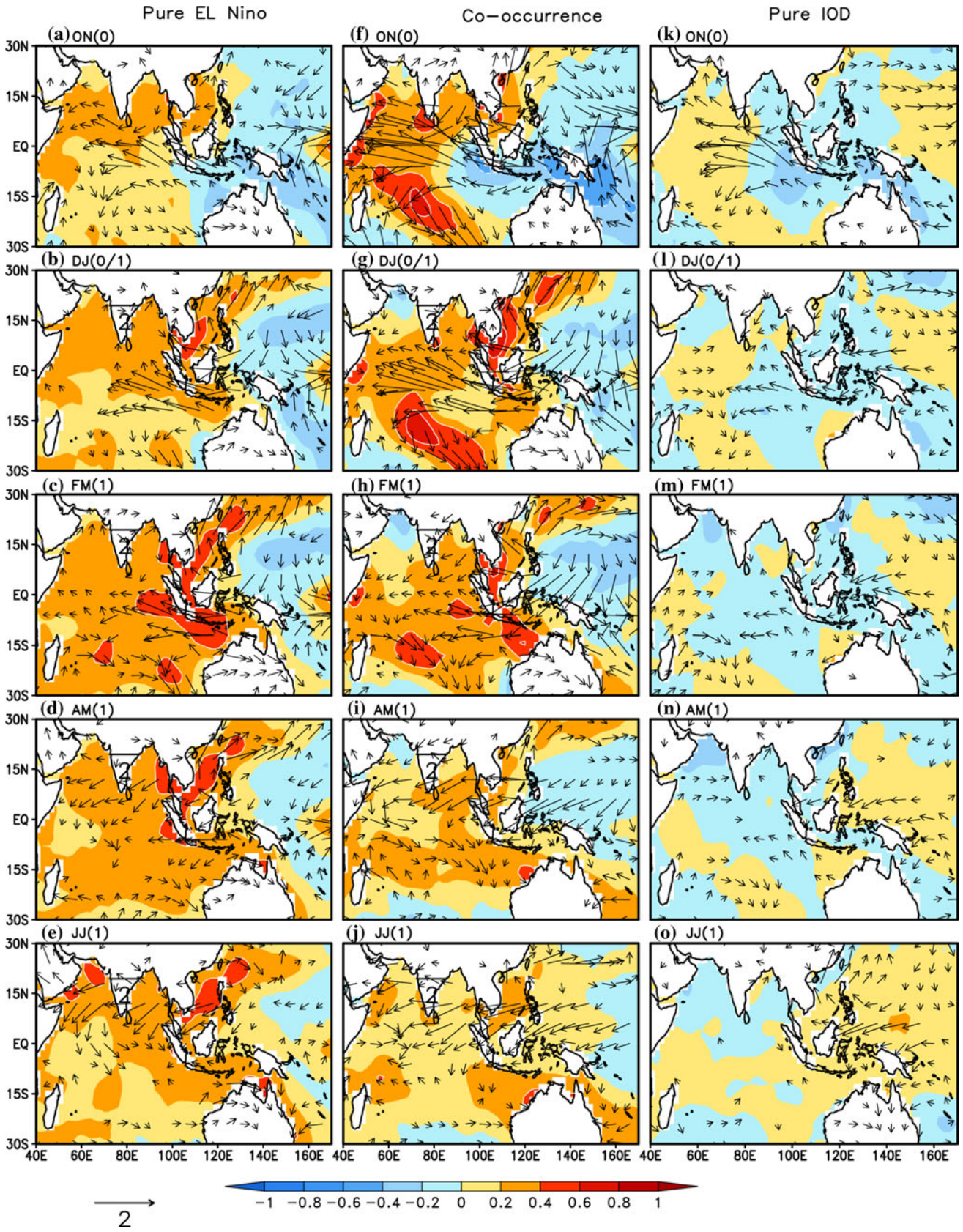

Fig. 3 Bimonthly composite of ER SST (*shaded*, °C, *white contours* indicate above ±0.4) and 20CR surface wind anomaly (*vectors*, ms^{-1}) for (**a**–**e**) pure El Niño (*left panel*), **f**–**j** co-occurrence (*middle panel*) and **k**–**o** pure IOD (*right panel*) years for the period of 1871–2008

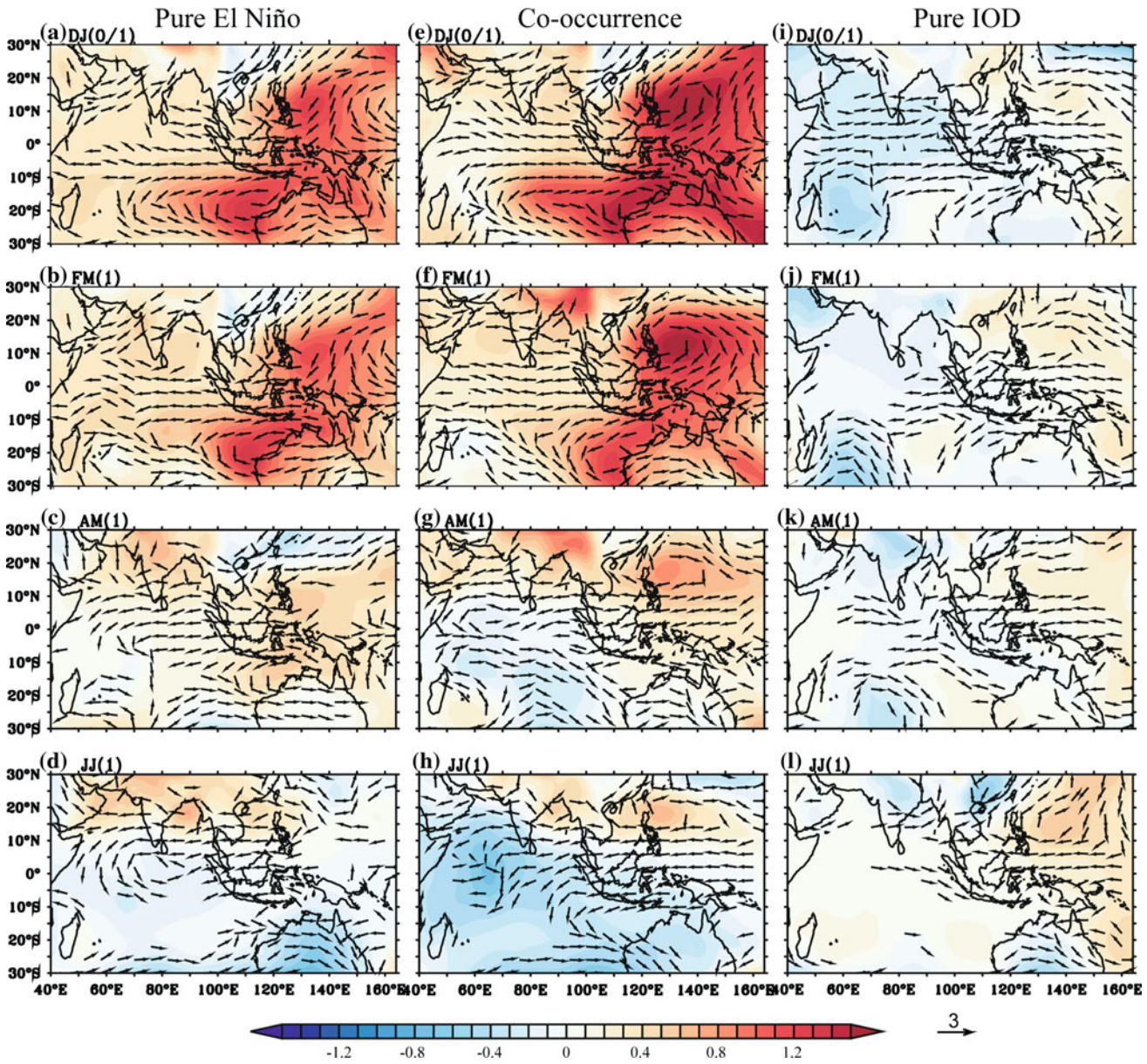

Fig. 4 Bimonthly composite of 20CR SLP anomalies (*shaded*, hPa) and 850 hPa wind anomalies (*vectors*, ms^{-1}) for (**a**–**d**) pure El Niño (*left panel*), **e**–**h** co-occurrence (*middle panel*) and **i**–**l** pure IOD (*right panel*) years for the period of 1871–2008

that asymmetric mode in surface winds is developed in AM(1) but persisted up to JJ(1) and is consistent with changes in SLP anomalies over the TIO (Fig. 4d). In co-occurrence years, the southeast Indian Ocean positive SLP anomaly weakens from FM(1) and is replaced by negative SLP anomalies by AM(1). The meridional SLP gradient over TIO is very prominent and well organized around the equator in AM(1). This shows that asymmetric mode in low level winds over TIO during spring is also controlled by meridional SLP gradient. The SLP gradient is weaker in co-occurrence composites during JJ(1) resulting very weak asymmetric mode. In pure IOD composites asymmetric mode is absent both in spring and summer over the TIO.

Rainfall anomalies over the TIO exhibit asymmetric pattern during spring as evident from the EOF analysis (Fig. 2). We present land precipitation and 20CR precipitable water content (PPW) (as a proxy for rainfall) to examine asymmetric mode in pure El Niño and co-occurrence years (Fig. 5). Pure IOD composites are not shown because of the absence of spring asymmetric mode. Over the northwest Pacific, large negative PPW anomalies associated with anticyclonic circulation is seen in DJ(0/1) for both pure El Niño and co-occurrence composites. Both 20CR and land rainfall anomalies show westward extension of negative anomalies from DJ(0/1) to AM(1). This westward extension is much more prominent and faster in

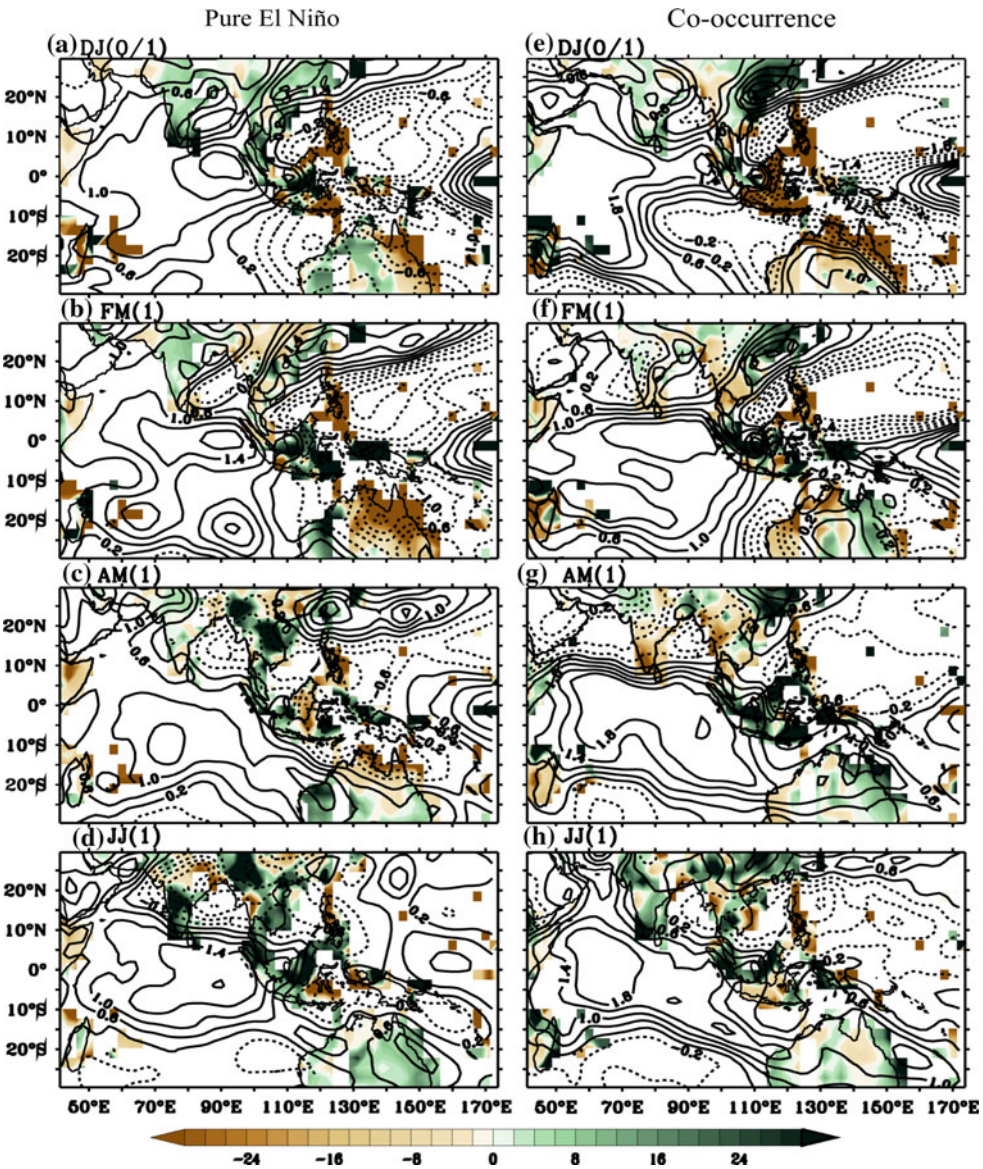

Fig. 5 Bimonthly composite of observed land precipitation anomalies (*shaded*, mm month^{-1}) and 20CR precipitable water content anomalies (*contours*, kgm^{-2} s^{-1}) for (**a**–**d**) pure El Niño (*left panel*) and **e**–**h** co-occurrence (*middle panel*) years for the period of 1871–2008

co-occurrence composites (Fig. 5). In co-occurrence years during FM(1) negative anomalies occupy over the Bay of Bengal and Indian land mass. In AM(1), this negative rainfall anomalies (Fig. 5g) extend over the entire north Indian Ocean and Indian land mass and asymmetric mode in rainfall pattern becomes very prominent. Land rainfall anomalies are negative over Philippines to southern tip of India and positive over the Seychelles islands. From AM(1) to JJ(1), rainfall anomalies over the north Indian Ocean change to positive in co-occurrence years with a weakening of asymmetric wind patterns. In case of pure El Niño composites asymmetric rainfall (PPW) and winds are weak as compared to co-occurrence years (Figs. 5c, g). Land rainfall shows large positive anomalies over Indian sub-continent during JJ(1). However, land rainfall changes during summer (following El Niño) are similar as discussed in earlier studies (e.g., Yang et al. 2007; Wu et al. 2008; Xie et al. 2009; Chowdary et al. 2011). In both pure El Niño and co-occurrence composites wind anomalies are easterlies in JJ(1) over the southern peninsular India. Easterly wind anomalies in summer generally weaken the mean southwesterlies. Rainfall increase over the south peninsula in spite of weak winds is due to moist processes, such as moist stability and moisture transport associated with the warm north Indian Ocean (Park et al. 2010). Weakening of low level winds lead to north Indian Ocean warming that in turn increases the monsoon rainfall by reducing the moist stability and increasing the horizontal moisture advection (Yang et al. 2007; Park et al. 2010).

The TIO displays coherent SST warming in both north and south of the equator during spring after peak phase of El Niño (Klein et al. 1999; Lau and Nath 2000, Alexander

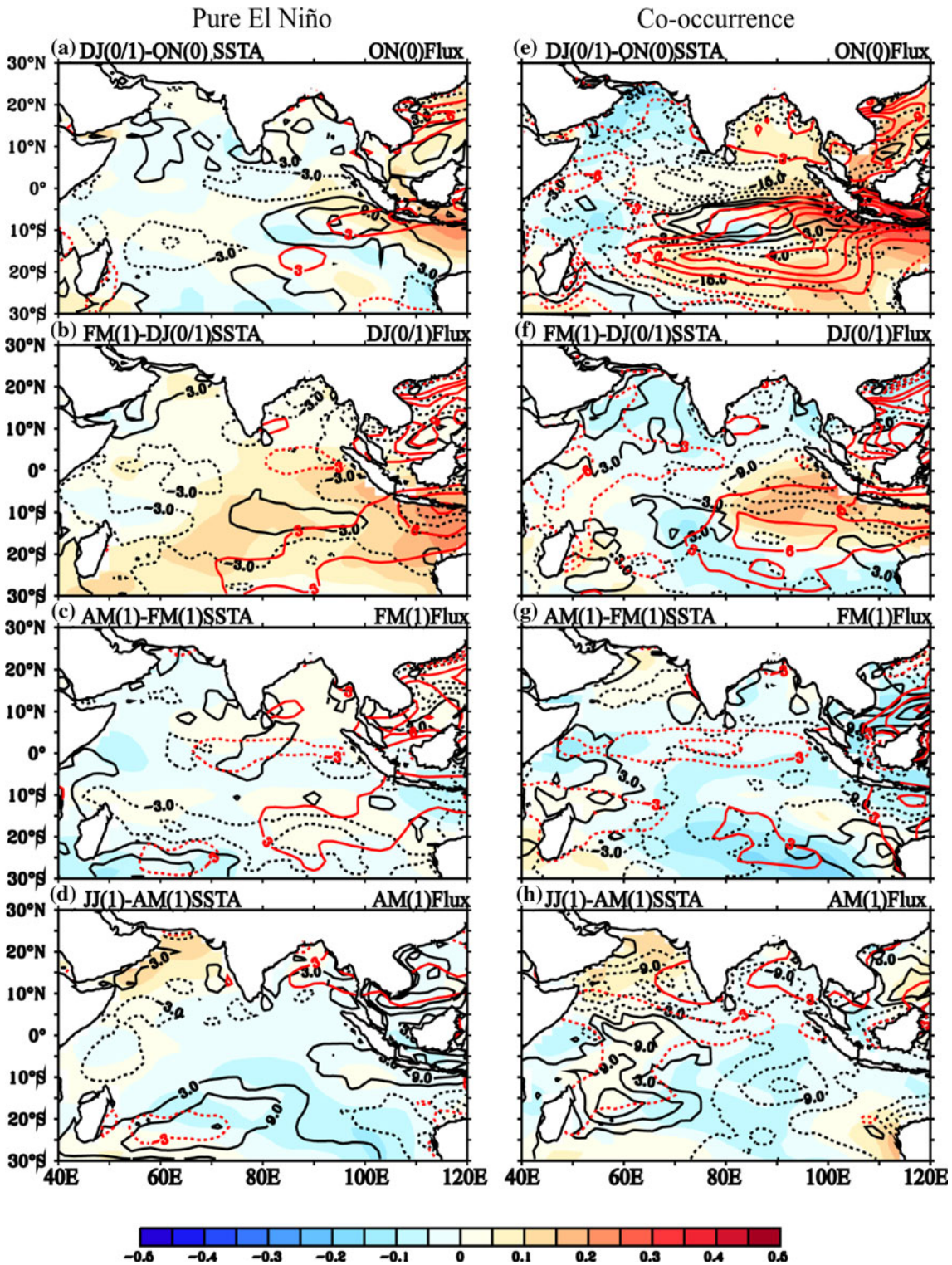

Fig. 6 Same as Fig. 5, but for bimonthly composite of ER SST tendency (*shaded*, °C month^{-1}), 20CR upward Latent Heat Flux anomaly (*black contours*, Wm^{-2}) and downward Short Wave radiation anomalies (*red contours*, Wm^{-2})

et al. 2002; Chowdary and Gnanaseelan 2007; Yang et al. 2007; Xie et al. 2002; Du et al. 2009). Variations in SST over the TIO play an important role in developing the asymmetric mode (Wu et al. 2008; Wu and Yeh 2010). Therefore, it is important to investigate the causes of changes in SST pattern during pure El Niño and co-occurrence years. Several studies pointed out the importance of heat flux in determining the SST variability during

decay phase of El Niño (Klein et al. 1999; Alexander et al. 2002; Chowdary and Gnanaseelan 2007, Du et al. 2009). Figure 6a–h show composite upward Latent Heat Flux (LHF) anomalies and downward Short Wave (SW) radiation anomalies and SST anomaly tendency (shaded) in pure El Niño and co-occurrence years. Though there are changes in the TIO SST pattern from ON(0) to JJ(1), warming is maintained in all seasons during pure El Niño composite (Fig. 3a–e). The changes in SST from ON(0) to DJ(0/1) are not much significant over the TIO (Fig. 6a) due to weak heat flux anomalies in ON(0). SST anomaly tendency is very significant from DJ(0/1) to FM(1) with enhanced warming in the entire TIO. The warming tendency is consistent (mainly) with LHF and to some extent with SW radiation particularly over southeast TIO. The strong warming of FM(1) continued into AM(1), however the SST tendency is very weak. In some regions SST tendency is controlled by both SW radiation and LHF (Fig. 6c). Significant changes in SST from AM(1) to JJ(1) are also influenced by LHF. In case of co-occurrence composite SST shows strong warming in east and cooling tendency in west TIO from ON(1) to DJ(0/1). Most of the SST changes in the western TIO are controlled by both LHF and SW radiation, whereas in the eastern TIO SW radiation is more dominant. SST changes from DJ(0/1) to AM(1) are mostly determined by heat fluxes (Fig. 6f–h) except over the southwest TIO. This supports the role of ocean dynamics (in the form of downwelling Rossby waves) in the southwest TIO warming.

Our results indicate that the homogeneous SST pattern in spring after pure El Niño years is governed by heat flux. In case of co-occurrence years, SST changes over the north Indian Ocean are controlled by heat flux and in southwest TIO both ocean dynamics and heat flux are important. These results are consistent with earlier studies (e.g., Chowdary and Gnanaseelan 2007). Cold SST anomalies north of the equator and warm anomalies in the south play an important role in developing the asymmetric mode (Wu et al. 2008).

5 Spring asymmetric mode in the atmospheric model simulations

It is very important to verify the role of changes in SST pattern and magnitude in developing spring asymmetric wind and precipitation over the TIO during co-occurrence and pure El Niño years. Forced with observed SST, CAM3 atmospheric GCM displayed good skills in simulating spring asymmetric mode in surface winds over the TIO during recent decades (Huang et al. 2010). To complement our observational analysis, we examined the ensemble

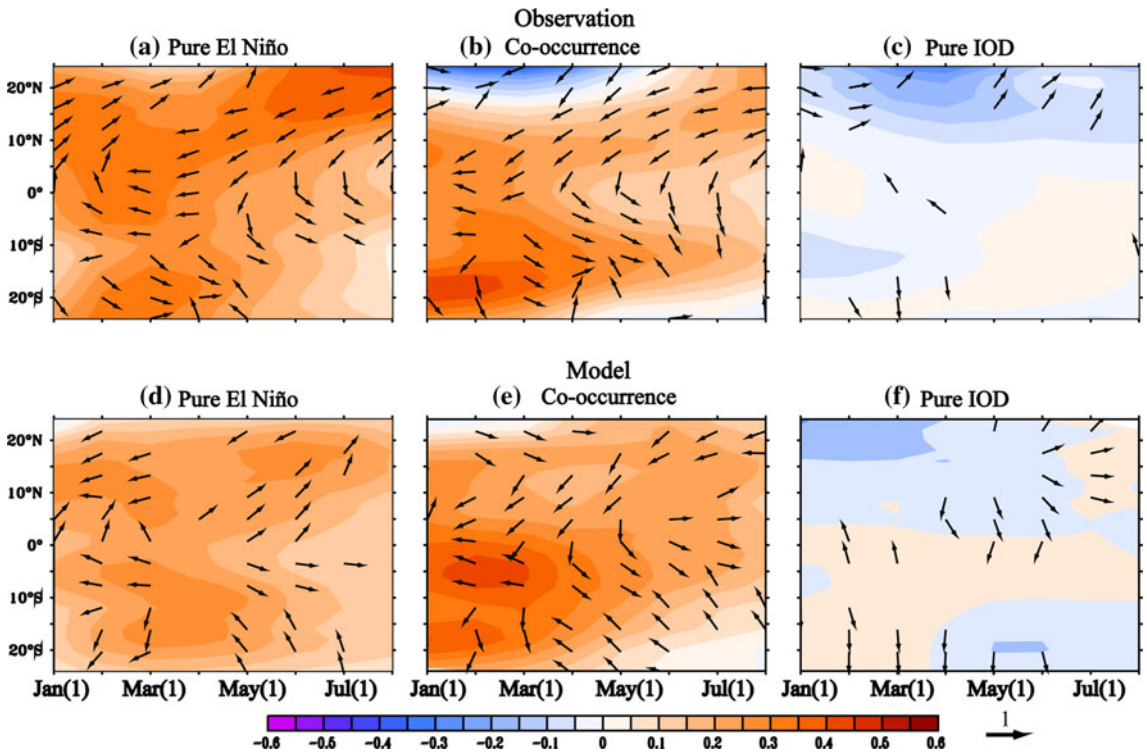

Fig. 7 Composite of SSTA (*shaded*, °C) and surface wind anomalies (*vectors*, m s^{-1}) average over 50–100°E for (**a**, **d**) pure El Niño (*left panel*), **b** and **e** co-occurrence (*middle panel*) and **c** and **f** pure IOD years (*right panel*) during the period of 1871–2000 for observation (*top panel*) and Model (*bottom panel*)

mean simulations (5 ensembles) from an AGCM forced with TOGA SST from 1871 to 2000. This model successfully reproduced the ENSO-Indo-western Pacific teleconnections in the El Niño decay phase, especially during summer (Chowdary et al. 2012). Figure 7 shows time-latitudinal plot of SST and surface wind anomaly composites during pure El Niño, co-occurrence and pure IOD years for both observations and model. Note that the model SST mentioned in Fig. 7 (top panels) is actually the observed SST which has been used to force the model. Minor differences found in the pattern of SST anomalies (between model and observations) are attributed to the source of different products. Large scale SST patterns in composites are similar in both the products. In the model, the asymmetric wind pattern (of spring) is well developed in co-occurrence composites (Fig. 7b, e) as in observations. During pure El Niño years the model failed to simulate asymmetric mode in spring. This indicates that the homogeneous SST warming prevents the development of asymmetric mode in spring. In case of co-occurrence composites, February to July, meridional gradient in the TIO SST plays important role in the evolution of spring asymmetric mode. The wind anomalies are very weak in pure IOD composites. Huang et al. (2010) suggests that meridional SST gradients during the epoch after mid-1970s contributed to the formation of wind pattern over the TIO. The SST gradients in the TIO are very weak in the epoch starting from 1950 to mid-1970 and hence the spring asymmetric modes in surface winds and precipitation are absent.

From DJ(0/1) to FM(1) model simulated SLP and precipitation are well comparable with 20CR and observed land rainfall over the Indo-western Pacific region (Fig. 8). Associated with SLP high and anticyclonic circulation over the northwest Pacific, strong negative rainfall anomalies are well reproduced by model from DJ(0/1) to JJ(1). Negative precipitation rate anomalies over the north Indian Ocean and positive anomalies over the southeast tropical Indian Ocean are also well simulated by model. During AM(1) a very weak SLP gradient (meridional) is observed over the TIO in pure El Niño composites (Fig. 8c) along with SST and this may be responsible for the absence of asymmetric wind and rainfall pattern in the TIO. The meridional gradient in SLP is well simulated by the model in the co-occurrence case and so is the case for asymmetric pattern in rainfall and surface winds. Model results support our argument that the meridional gradient in SLP and SST is very important for developing spring asymmetric mode. The northwest Pacific high induced northeasterlies in the north Indian Ocean are also important for maintaining spring asymmetric pattern over the TIO (Huang et al. 2010). However, model has limited skills in simulating westward extension of the northwest Pacific high. Earlier studies demonstrated that the antisymmetric wind pattern is anchored by the positive SST and precipitation anomalies in the southwest TIO (Du et al. 2009; Wu and Yeh 2010; Huang et al. 2010; Xie et al. 2010). Our analysis shows that strong positive SST anomalies of spring in the southwest TIO is responsible for the enhanced convection over that region during co-occurrence composites. Convection is relatively weaker in pure El Niño years. From AM(1) to JJ(1), changes in SLP and rainfall patterns in response to observed SST are well represented by the model during both El Niño and co-occurrence years (Figs. 8d–h).

6 Asymmetric mode in station and ship track data

In order to reconfirm our results, we carried out similar composite analysis at two stations, one to the north of the equator (Colombo 6.90°N, 79.90°E) and the second one to the south of equator (Seychelles 4.70°S, 55.50°E) in addition to the ship track data. Figure 9 shows the composite of monthly total precipitation anomaly (upper panel) and air temperature anomaly (bottom panel) over these two stations. In the pure El Niño case, the asymmetric pattern is observed in AM(1) with positive precipitation anomaly over Seychelles and negative precipitation anomaly over Colombo. However during co-occurrence years the asymmetry in precipitation is seen from February(1) onwards and is much more prominent as compared to pure El Niño composite. Air temperature also reveals similar asymmetric pattern (as in precipitation anomalies). Strong positive air temperature anomalies over Colombo and negative temperature anomalies over Seychelles are seen during co-occurrence years, whereas this gradient is much weaker during pure El Niño case. Ship track observations over the north Indian Ocean also displays northeasterly wind anomalies both in pure El Niño and co-occurrence composites. SST over the north Indian Ocean is warmer during the decay phase of pure El Niño and is apparent in both reanalysis and ship track data (Fig. 10). Weak SST anomalies in the Arabian Sea from February to April are also evident in ship observations. Similar to reanalysis data, SLP over the north Indian Ocean turned to positive (from negative) in early summer during co-occurrence years in ship observations. In case of pure El Niño years positive SLP anomalies persisted to early summer in both data sets. In pure IOD years, SST and SLP anomalies are weak in the following spring. Overall, the conclusions made from the reanalysis data and model are supported by ship and station data.

7 Summary and discussion

We have used twentieth century reanalysis (20CR), atmospheric model simulations and in situ observations to

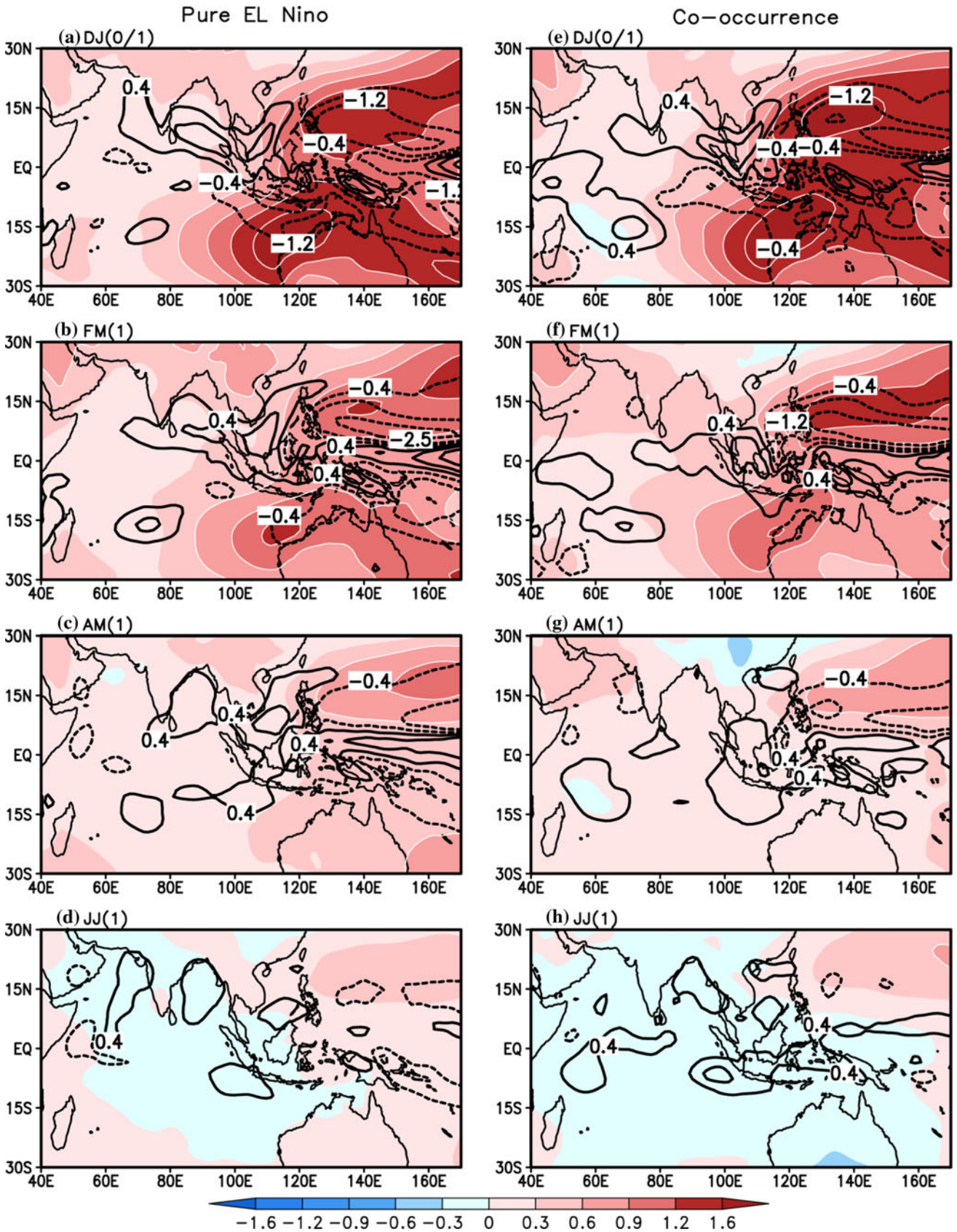
Pure EL Nino
Co−occurrence
(a) DJ(0/1)
(b) FM(1)
(c) AM(1)
(d) JJ(1)
(e) DJ(0/1)
(f) FM(1)
(g) AM(1)
(h) JJ(1)
30N
15N
EQ
15S
30S
40E
60E
80E
100E
120E
140E
160E
−1.6 −1.2 −0.9 −0.6 −0.3 0 0.3 0.6 0.9 1.2 1.6

◄ **Fig. 8** Bimonthly composite (for period of 1871–2000) of model SLP (*shaded*, hPa, *white contours* indicate above ±0.6) and model Precipitation rate anomalies (*contours*, mm day^{-1}) for pure El Niño (*left panel*), co-occurrence (*middle panel*) and pure IOD (*right panel*) years. Contour interval for precipitation is 0.2

examine the evolution of asymmetric wind and precipitation pattern over the TIO during spring after peak phase of El Niño and IOD years. During boreal spring asymmetric pattern in rainfall (surface winds) develops with negative (northeasterly) anomalies north of the equator and positive (northwesterly) anomalies in the south during the decay phase of El Niño (Kawamura et al. 2001; Wu et al. 2008). The spring asymmetric mode is one of the important component in developing the north Indian Ocean warming in summer and this warming is found to display large impact on the Asian monsoon circulation (Yang et al. 2007; Xie et al. 2009, 2010), Based on observations, Wu et al. (2008) demonstrated that the asymmetric mode is closely related to ENSO and IOD. However, the relative role of El Niño and IOD in developing spring asymmetric mode over the TIO is not clear from the previous studies. Therefore, the present study is focused on understanding the impact of El Niño and IOD forcing on the spring asymmetry in wind and rainfall.

Our results from reanalysis data reveals that the spring asymmetric mode is well developed when El Niño co-occurred with IOD, but is very weak during the pure El Niño events and is absent in pure IOD composites. Northeasterly winds to the north of the equator are present from FM(1) but northwesterlies to south is very weak in pure El Niño composites and develops only in AM(1). Asymmetric mode in precipitation anomaly pattern is also not well developed during pure El Niño events and only observed in late spring. Persistent northwest Pacific anticyclone from DJ(0/1) to JJ(1) induces the northeasterlies in the north Indian Ocean in spring. The difference between co-occurrence and pure El Niño composites in developing asymmetric mode is basically due to the differences in the TIO SST and SLP patterns. Both surface heat flux and ocean dynamics play important role in maintaining the meridional SST gradient over the TIO and hence in SLP during the co-occurrence years. In case of pure El Niño composites the TIO SST is more homogeneous in space, which suppresses the SLP gradients. In case of co-occurrence years the SST anomalies show a strong north–south gradient from DJ(0/1) to AM(1). North Indian Ocean displays cooling in this period. Regressed wind anomalies over Indian Ocean with two indices (separately) based on TIO meridional SST gradient (the difference between the SST anomalies averaged over 25°S to 5°S, 55°E to 80°E and 10°N to 25°N, 50°E to 75°E for FM) and northwest Pacific anticyclone (SLP anomalies average over 5°N to 25°N and 120°E to 150°E for both the FM and AM) revealed that the meridional SST gradient over the Indian Ocean mainly generates the asymmetry in wind pattern in FM(1) and the northwest Pacific anticyclone maintains it in AM(1) by inducing the northeasterly wind anomalies into north Indian Ocean. Partial correlation analysis also supports this result. The northwest Pacific high is somewhat stronger during co-occurrence composites compared to pure El Niño composites. This difference may also play some role in strengthening the northeasterlies over the

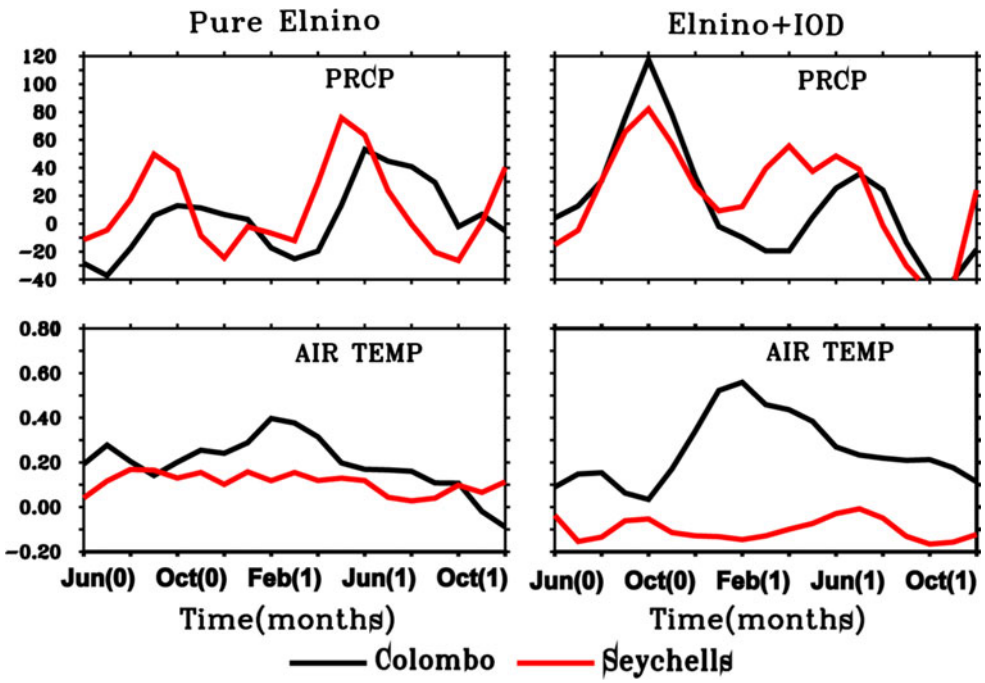

Fig. 9 Composite of monthly total precipitation anomalies (10^{-1} mm month^{-1}, *top panel*) and air temperature anomaly (°C, *bottom panel*) for pure El Niño (*left panel*) and co-occurrence (*right panel*) over Colombo (*black line*) and Seychelles (*red line*)

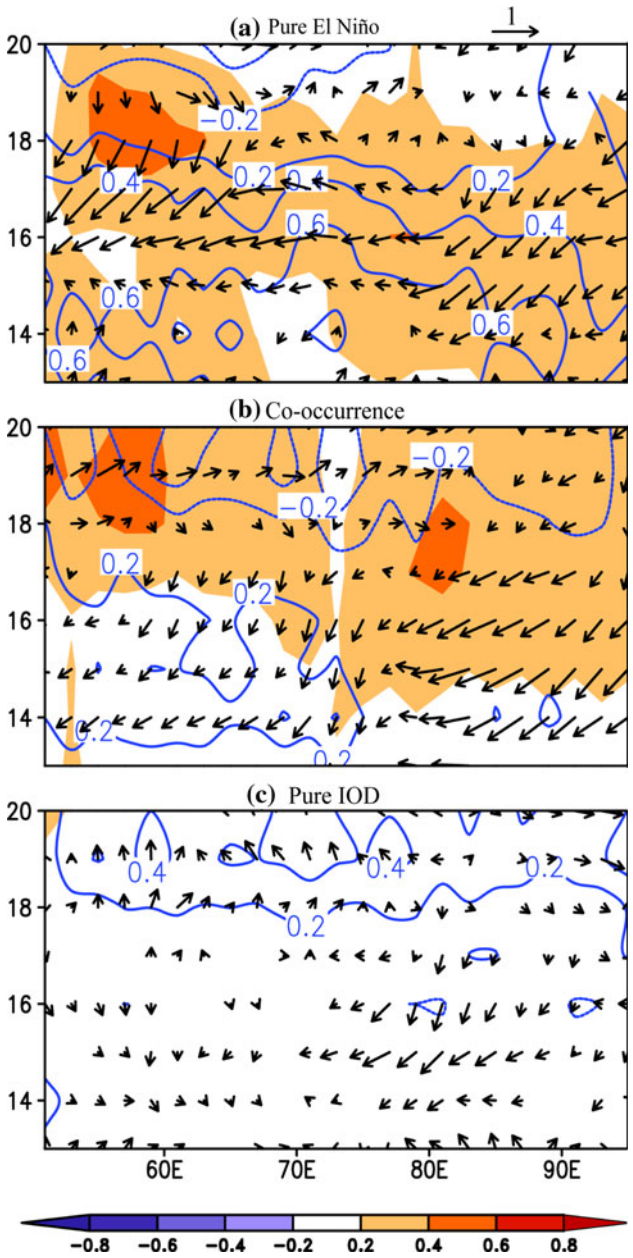

Fig. 10 Time-longitude plot of composite of north IO SST anomalies (*shaded*, °C), surface wind anomalies (*vectors*, ms^{-1}) and SLP anomalies (*contours*, hPa) (alone ship track) for pure El Niño (*top panel*), co-occurrence (*middle panel*) and pure IOD (*bottom panel*) years

north Indian Ocean in spring during co-occurrence years. Our results show that this spring asymmetric mode is strongly associated with the SLP anomalies. In pure IOD composites SST and wind anomalies are strong only during ON(0) and DJ(0/1) and are very weak in FM(1) and AM(1).

Here we used about 140 years of long dataset to demonstrate the asymmetric mode. To investigate the response of TIO SST to the surface circulation and precipitation anomalies we have analyzed CAM3 TOGA run during the period of 1871–2000. In the model, this asymmetric spring wind pattern is well developed in co-occurrence composites but absent in pure El Niño events. Westward extension of northeasterly wind anomalies are very weak in model compared to reanalysis. The atmospheric GCM results support our hypothesis that the meridional gradient in SST over the TIO is very important in developing asymmetric mode in winds and precipitation along with SLP. Further, analysis of station and ship data confirmed the above results. Our observational and model results show that spring asymmetric wind and precipitation pattern over the TIO are well developed when El Niño co-occurred with IOD, which is mainly due to the meridional SST and SLP gradients and stronger northwest Pacific anticyclonic circulation.

Acknowledgments Soumi acknowledges the support of Council of Scientific and Industrial Research (CSIR), India for Junior Research Fellowship. We thank INCOIS, Hyderabad and Prof. B. N Goswami, Director IITM for support. We thank H. Tokinaga and S-P Xie for providing ship track data and Bin Wang for scientific discussion. The comments from two anonymous reviewers have helped us to improve the manuscript. ER SST data is provided by the NOAA/OAR/ESRL PSD, Boulder, Colorado, USA. Yuko M. Okumura, Clara Deser, Adam Phillips of the CESM (Community Earth System Model) Climate Variability Working Group for making the CAM3 TOGA simulations available. Figures are prepared in ferret and GrADS.

References

Alexander MA, Bladé I, Newman M, Lanzante JR, Lau N-C, Scott JD (2002) The atmospheric bridge: the influence of ENSO teleconnections on air–sea interaction over the global oceans. J Clim 15:2205–2231

Chambers DP, Tapley BD, Stewart RH (1999) Anomalous warming in the Indian Ocean coincident with El Niño. J Geophys Res 104:3035–3047

Chowdary JS, Gnanaseelan C (2007) Basin-wide warming of the Indian Ocean during El Niño and Indian Ocean dipole years. Int J Climatol 27:1421–1428

Chowdary JS, Gnanaseelan C, Xie S-P (2009) Westward propagation of barrier layer formation in the 2006–07 Rossby wave event over the tropical southwest Indian Ocean. Geophys Res Lett 36:L04607. doi:10.1029/2008GL036642

Chowdary JS, Xie S-P, Lee J-Y, Kosaka Y, Wang B (2010) Predictability of summer Northwest Pacific climate in eleven coupled model hindcasts: local and remote forcing. J Geophys Res Atmos 115:D22121. doi:10.1029/2010JD014595

Chowdary JS, Xie S-P, Luo J-J, Hafner J, Behera S, Masumoto Y, Yamagata T (2011) Predictability of Northwest Pacific climate during summer and the role of the tropical Indian Ocean. Clim Dyn 36:607–621. doi:10.1007/s00382-009-0686-5

Chowdary JS, Xie S-P, Tokinaga H, Okumura YM, Kubota H, Johnson NC, Zheng X-T (2012) Inter-decadal variations in ENSO teleconnection to the Indo-western Pacific for 1870–2007. J Clim 25:1722–1744

Collins WD et al (2006) The formulation and atmospheric simulation of the community atmosphere model version 3 (CAM3). J Clim 19:2144–2161

Compo GP, Whitaker JS, Sardeshmukh PD, Matsui N, Allan RJ, Yin X, Gleason BE, Vose RS, Rutledge G, Bessemoulin P, Brönnimann S, Brunet M, Crouthamel RI, Grant AN, Groisman PY, Jones PD, Kruk MC, Kruger AC, Marshall GJ, Maugeri M, Mok HY, Nordli Ø, Ross TF, Trigo RM, Wang XL, Woodruff SD, Worley SJ (2011) The twentieth century reanalysis project. Q J R Meteorol Soc 137:1–28

Dai A, Fung IY, Del Genio AD (1997) Surface observed global land precipitation variations during 1900–1988. J Clim 10:2943–2962

Du Y, Xie S-P, Huang G, Hu K-M (2009) Role of air–sea interaction in the long persistence of El Niño-induced North Indian Ocean warming. J Clim 22:2023–2038

Gill AE (1980) Some simple solutions for heat-induced tropical circulation. Q J R Meteorol Soc 106:447–462

Huang G, Hu K, Xie S-P (2010) Strengthening of Tropical Indian Ocean teleconnection to the Northwest Pacific since the Mid-1970s: an atmospheric GCM study. J Clim 23:5294–5304

Hurrell JW, Hack JJ, Shea D, Caron JM, Rosinski J (2008) A new sea surface temperature and sea ice boundary data set for the community atmosphere model. J Clim 21:5145–5153

Kawamura R, Matsuura T, Iizuka S (2001) Role of equatorially asymmetric sea surface temperature anomalies in the Indian Ocean in the Asian summer monsoon and El Niño–southern oscillation coupling. J Geophys Res 106:4681–4693

Klein SA, Soden BJ, Lau NC (1999) Remote sea surface temperature variations during ENSO: evidence for a tropical atmospheric bridge. J Clim 12:917–932

Lau NC, Nath MJ (2000) Impact of ENSO on the variability of the Asian-Australian monsoons as simulated in GCM experiments. J Clim 13:4287–4309

Lau NC, Nath MJ (2003) Atmosphere-ocean variations in the Indo-Pacific sector during ENSO episodes. J Clim 16:3–20

Masumoto Y, Meyers G (1998) Forced Rossby waves in the southern tropical Indian Ocean. J Geophys Res 103:27589–27602

Meyers G, McIntosh P, Lidia P, Mike P (2007) The Years of El Niño, La Niña, and Interactions with the Tropical Indian Ocean. J Clim 20:2872–2880

Murtugudde R, McCreary JP, Busalacchi AJ (2000) Oceanic processes associated with anomalous events in the Indian Ocean with relevance to 1997–1998. J Geophys Res 105:3295–3306

Nigam S, Shen HS (1993) Structure of oceanic and atmospheric low-frequency variability over the tropical Pacific and Indian oceans. Part I: COADS observations. J Clim 6:657–676

Park H-S, Chiang JCH, Lintner BR, Zhang GJ (2010) The delayed effect of major El Niño events on Indian monsoon rainfall. J Clim 23:932–946

Perigaud C, Delecluse P (1993) Annual sea-level variations in the tropical Indian Ocean from GEOSAT and shallow water simulations. J Geophys Res 97:20169–20179

Saji NH, Goswami BN, Vinayachandran PN, Yamagata T (1999) A dipole mode in the tropical Indian Ocean. Nature 401:360–363

Shinoda T, Alexander MA, Hendon HH (2004) Remote response of the Indian Ocean to interannual SST variations in the tropical Pacific. J Clim 17:362–372

Smith TM, Reynolds RW (2004) Improved extended reconstruction of SST (1854–1997). J Clim 17:2466–2477

Tokinaga H, Tanimoto Y (2004) Seasonal transition of SST Anomalies in the Tropical Indian Ocean during El Niño and Indian Ocean Dipole years. J Meteorol Soc Jpn 82:1007–1018

Wang B, Wu R, Fu X (2000) Pacific-east Asian teleconnection: how does ENSO affect East Asian climate? J Clim 13:1517–1536

Webster PJ, Moore AM, Loschnigg JP, Leben RR (1999) Coupled oceanic-atmospheric dynamics in the Indian Ocean during 1997–1998. Nature 401:356–360

Wu R, Yeh S-W (2010) A further study of the tropical Indian Ocean asymmetric mode in boreal spring. J Geophys Res 115:D08101. doi:10.1029/2009JD012999

Wu R, Kirtman BP, Krishnamurthy V (2008) An asymmetric mode of tropical Indian Ocean rainfall variability in boreal spring. J Geophys Res 113:D05104. doi:10.1029/2007JD009316

Xie P, Arkin PA (1996) Analyses of global monthly precipitation using gauge observations, satellite estimates, and numerical model predictions. J Clim 9:840–858

Xie S-P, Philander SGH (1994) A coupled ocean atmosphere model of relevance to the ITCZ in the eastern Pacific. Tellus 46A:340–350

Xie S-P, Annamalai H, Schott FA, McCreary JP (2002) Structure and mechanisms of South Indian Ocean climate variability. J Clim 15:864–878

Xie S-P, Hu K, Hafner J, Tokinaga H, Du Y, Huang G, Sampe T (2009) Indian Ocean capacitor effect on Indo-Western Pacific climate during the summer following El Niño. J Clim 22:730–747

Xie S-P, Du Y, Huang G, Zheng X-T, Tokinaga H, Hu K, Liu Q (2010) Decadal shift in El Niño influences on Indo-western Pacific and East Asian climate in the 1970s. J. Climate 23:3352–3368

Yang J, Liu Q, Xie S-P, Liu Z, Wu L (2007) Impact of the Indian Ocean SST basin mode on the Asian summer monsoon. Geophys Res Lett 34:L02708. doi:10.1029/2006GL02857